

# Tuning mesoporous molecular sieve SBA-15 for the immobilization of $\alpha$ -amylase

Sreedharan Ajitha · Sankaran Sugunan

Published online: 21 November 2009  
© Springer Science+Business Media, LLC 2009

**Abstract** The present work describes the immobilization of  $\alpha$ -amylase over well ordered mesoporous molecular sieve SBA-15 with different pore diameters synthesized by post synthesis treatment (PST) hydrothermally after reaction at 40°C. The materials were characterized by N<sub>2</sub> adsorption–desorption studies, small angle X-ray diffraction, scanning electron microscopy and high resolution transmission electron microscopy. Since  $\alpha$ -amylase obtained from *Bacillus subtilis* has dimensions of 35 × 40 × 70 Å it is expected that the protein have access to the pore of SBA-15 (PST-120°C) with diameter 74 Å. The pore dimension is appropriate to prevent considerable leaching. The rate of adsorption of the enzyme on silica of various pore sizes revealed the influence of morphology, pore diameter, pore volume and pH.

**Keywords** Immobilization · SBA-15 · Hydrothermal ·  $\alpha$ -Amylase · Adsorption

## 1 Introduction

Rapidly developing interface of chemistry and biology highlights the significance of catalysis which is further exemplified by the developments in material science like the invention of mesoporous and nanomaterials. Stabilized enzymes are of primary importance in a wide variety of scientific and industrial sectors, ranging from pharmaceutical formulations, to bioreactors and biosensors. The soft chemistry derived surfactant templated mesoporous

materials are the appropriate class of materials for enzyme immobilization as the perfectly ordered mesoporous silica is a material that could come close to providing a homogeneous environment with a large pore system [1].

Nature's catalyst is of nanometer scale and fixing them to nanopores of mesomaterials is an interesting task. However, recent theoretical models suggest that stabilization of proteins against unfolding can be achieved by physical confinement inside relatively small cages. This stabilization effect is attributed to the fact that in such confined spaces the unfolded configurations of the chain are not thermodynamically favored [2, 3]. Surfactant templated synthesis of silica has played an important role in the field of materials during the last decade. Zhao et al. [4, 5] extended the family of highly ordered mesoporous silicates by synthesizing Santa Barbara Amorphous (SBA) type materials, having uniform and adjustable pore size, thick pore wall, superior hydrothermal/thermal/mechanical stability, high surface area, pore volume, and open pore structure. The pore size of the mesochannels should be sufficiently large for comfortable entrapment of bimolecules [6, 7]. Balkus et al. [8] were the first to explore nanoporous silica for enzyme immobilization. A number of enzymes have been immobilized on nanoporous MCM-41, SBA-15 and silica based porous materials. The influences of pore size, surface properties, pore structure and morphology of the supports on enzyme loading and activity has been reported [9–12]. Thermo stable  $\alpha$ -amylase from *Bacillus* species are of great industrial importance in the production of corn syrup or dextrose. Polylactic acid synthesized from corn syrup is in turn used for a multitude of applications including biodegradable sutures, biocompatible fibers, packaging, and functional replacements for commodity plastics such as styrene [13]. According to the reports of Sugunan et al. [14–16], complete entrapment of

S. Ajitha · S. Sugunan (✉)  
Department of Applied Chemistry, Cochin University of Science and Technology, Cochin, Kerala 22, India  
e-mail: ssg@cusat.ac.in

$\alpha$ -amylase onto inorganic porous materials was not possible due to inappropriate pore sizes. Pandya et al. [17] investigated adsorption on functionalized SBA-15. However, the material was of low quality as the synthesis was done at room temperature. To study the effect of pore size on protein adsorption and to compare the activity of enzymes entrapped in various pore sizes, perfectly ordered mesoporous materials with similar framework is the primary requirement. Most of the authors have compared the protein adsorption on different pore sizes of MCM-41 and SBA-15 with entirely different frame works. There are only very few reports with SBA-15 of various pore sizes. We have prepared SBA-15 materials with various pore sizes by post synthesis heat treatment hydrothermally after reaction at 40°C resulting in ordered mesoporous materials. The pore diameters of the samples were sufficient to encapsulate  $\alpha$ -amylase of hydrodynamic radius  $35 \times 40 \times 70 \text{ \AA}$ . The activity of immobilized enzymes was compared in different pore sizes, since confinement of enzyme in size matching pore can restrain enzyme unfolding or denaturation. It has been found that the amount of adsorption mainly depends on the solution pH as well as the pore volume, pore diameter and morphology of the mesoporous silica. The activity increased with the increase of pore size as the substrate and products can easily enter in and out of the pore.

## 2 Experimental

Siliceous SBA-15 was synthesized according to the procedure reported by Zhao et al. [4]. In a typical synthesis procedure, 2 g of P123 (pluronic) surfactant was stirred with 20 ml of deionized water at 40°C. The mixture was stirred till the surfactant gets dissolved, followed by the slow addition of 30 g of 2 M HCl solution. The stirring was then continued for 30 min and 4.5 g of TEOS were added to the solution drop wise. The mixture was stirred for another 24 h and autoclaved at, 100,120 and 130°C for 48 h (samples denoted as S-1, S-2, and S-3). The solid material was then filtered, washed with water and acetone, air dried and calcined at 550°C for 6–8 h.

The powder X-ray diffraction (XRD) measurements were carried out on a Bruker D8 Advance Diffractometer at 40 kV and 30 mA using a Cu K $\alpha$  radiation. The isotherms of nitrogen adsorption–desorption were measured at liquid nitrogen temperature using a Micromeritics Tristar 3000 surface area analyzer. The surface-area measurement is based on the BET method, the pore size distributions and the pore diameter were calculated using BJH approach. For enzyme loaded samples during the sample preparation degassing was done at room temperature in N<sub>2</sub> atmosphere for 12–16 h prior to surface area measurements. It was also

compared with a blank degassed under same conditions. Scanning electron microscopy (SEM) micrographs were obtained using JEOL-JSM-6300 operating at an accelerating voltage of 20–30 kV after samples were sputtered with a thin layer of Au. High resolution transmission electron microscopy (HRTEM), images was recorded on JEOL 2010 F and Philips CM200 FEG with an acceleration voltage of 20 kV.

Adsorption experiments were carried out by contacting 100 mg of samples with different pore diameters with a protein concentration of 3 mg/ml. Phosphate buffer (0.1 M, pH 6–8) and phthalate buffer (0.1 M, pH 4–5) were used as the medium during the adsorption process (samples denoted as S-1e<sub>1</sub>, S-2e<sub>1</sub>, S-3e<sub>1</sub>). The adsorbent and enzyme solution were shaken at 150 rpm in a temperature-controlled shaker at 25°C for 120 min. The filtrate after collecting at definite intervals was centrifuged for 10 min at 15,000 rpm. Activity of the enzymes attached to the pores of various dimensions was compared in a batch reactor using 3% starch solution at pH 6. Test for leaching of enzyme from supports was conducted by shaking the supported enzyme for 2 h at 25°C in 20 ml buffer solution of pH 6.

The enzyme protein in the supernatant liquid was estimated using the spectrometric method of Lowry et al. A standard curve was constructed using known amounts of BSA (Bovine Serum Albumin). Reagents required for the essay are (A) 2% solution of Na<sub>2</sub>CO<sub>3</sub> in 0.1 NaOH, (B) 0.5% solution of CuSO<sub>4</sub> in 1% Rochelle salt. (C) Mixture of 1 ml reagent B and 50 ml reagent A (D) Dilute Folin-Ciocalteu reagent with equal volume water. For the protein essay 1 ml enzyme was mixed with 5 ml of C and incubated for 10 min. Then 0.5 ml of the Folin-Ciocalteu reagent was added to the above mixture, shaken thoroughly and incubated for 30 min. Read the absorbance at 660 nm.

## 3 Results and discussion

### 3.1 Small angle XRD

The small angle XRD patterns of the calcined samples are presented in Fig. 1a. The intensity of d<sub>100</sub> reflection of S-1 exhibits three well-resolved peaks characteristic of SBA-15, a very intense peak at 2 $\theta$  of 0.894 and two distinct weak peaks between 1.56 and 1.78. These diffraction signals are indexable as (100), (110) and (200) reflections associated with p6 mm hexagonal symmetry, which is characteristic of SBA-15 materials [4]. The high-intensity (100) peak reflects a d-spacing of 100.4 Å and the succeeding peaks have d-values 57.36 Å (110) and 49.37 Å (200) consistent with a 2D hexagonal arrangement of the pores with a unit-cell parameter  $a = 115.9 \text{ \AA}$  at d (100). The diffractions due to all planes are clearly evident in the patterns of S-2

**Fig. 1** XRD patterns of SBA-15 **a** at temperatures 100, 120 and 130°C, **b** after immobilization on S-2

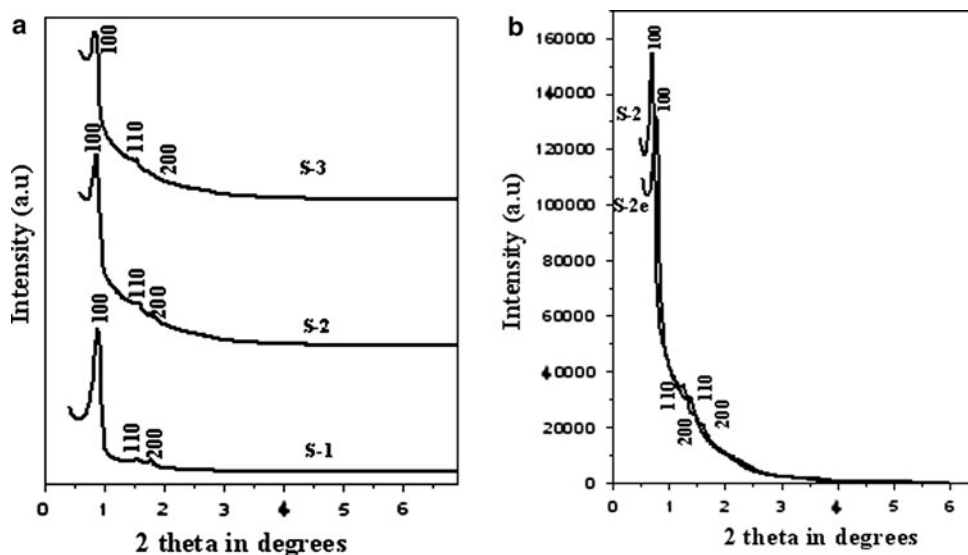


**Table 1** XRD results of silica of various pore dimensions used for protein adsorption studies

Sample	$d_{100}$ (Å)	$a_0$ (Å)	Wall thickness (Å)
S-1	100.4	115.9	52.9
S-2	105.9	122.3	48.3
S-3	109.8	126.9	42.9

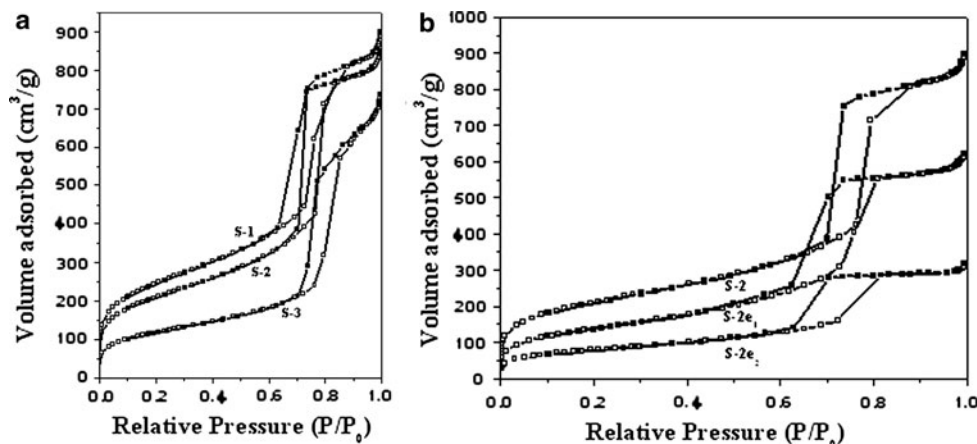
and S-3. The shift of  $2\theta$  to lower values indicates a change in unit cell parameter (Fig. 1a). The  $d$  (100) values and the calculated unit cell parameters ( $a_0 = 2d/\sqrt{3}$ ) are shown in Table 1. Both  $d$ -spacing and unit cell parameter increases with increase in ageing temperature [18]. Presence of all the peaks for immobilized samples confirms that the hexagonal structure is retained after the enzyme incorporation (Fig. 1b). Adsorption of enzyme decreases the intensity of all peaks compared to the parent SBA-15. This indicates

that the incorporation of enzyme slightly disturbs the ordered nature of SBA-15 and is due to the large contrast in density between the silica walls and the empty pores relative to that between the silica walls and the pores filled with  $\alpha$ -amylase molecules [19–21]. The slight change in  $d$ -spacing after immobilization in S-2 is because of the disordering in the pore channels or the strain arising as a result of the confined enzyme molecules.

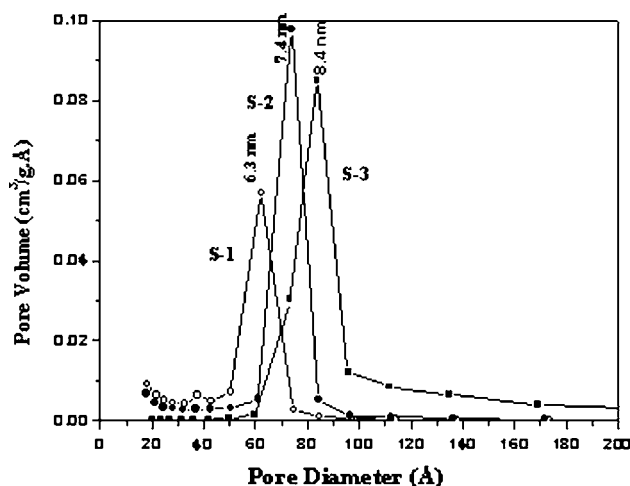
### 3.2 Nitrogen adsorption–desorption studies

Figure 2a shows the nitrogen adsorption–desorption isotherms for different SBA-15 silica samples. It is observed that all the isotherms are of type IV in nature as per IUPAC classification and exhibiting H1-type broad hysteresis loop which is characteristic of large pore mesoporous materials with uniform cylindrical channels [22]. These results can be

**Fig. 2** Nitrogen adsorption–desorption isotherms of SBA-15 **a** at temperatures 100, 120 and 130°C, **b** after enzyme immobilization on S-2 with different loading



attributed to capillary condensation taking place within a narrow range of tubular pores. The sharpness of the adsorption–desorption branches (located at a relative pressure from 0.6 to 0.8) indicates a narrow mesopore size distribution, and characteristic of good quality SBA-15. SBA-15 framework has been classified as an array of mesopore micropore network instead of an array of uniform mesoporous network. Several detailed structural elucidation studies on SBA-15 has confirmed the existence of micropores within the pore walls [23]. The ratio of micro-/mesoporosity in SBA-15 materials can be easily tuned by changing SBA-15 preparation conditions [24]. It is evident that elevated ageing temperature during synthesis has two consequences: it increases the pore size of the SBA-15 materials and decreases the fraction of microporosity present in the pores. An increase in the synthesis temperature and the temperature of the following hydrothermal treatment of the silicate-surfactant mesophase has a negative influence on micropore area and wall thickness. In this case the increase of synthesis temperature to 40°C and the hydrothermal treatment at high temperatures at 100, 120 and 130°C has reduced the microporosity. The reduction of microporosity in samples at higher temperature is confirmed by the fact that the linear region of the  $t$ -plot can be extrapolated to a very low intercept as shown in Fig. 4. The calculated  $WS_p/V_p$  values for different samples along with micropore volume and micropore area from  $t$ -plot are compiled in Table 2. The values are in close agreement with the theoretical values. But the values show large deviation from earlier experimental reports (which are 5–10 for SBA-15 type materials). The factor  $WS_p/V_p$  is theoretically expected to be 4 for cylindrical and 4.2 for hexagonal pores [25–27]. It is the geometric relation between the specific pore volume and the pore size of an infinite array of cylindrical pores arranged in



**Fig. 3** Pore size distribution from BJH of samples at different ageing temperatures

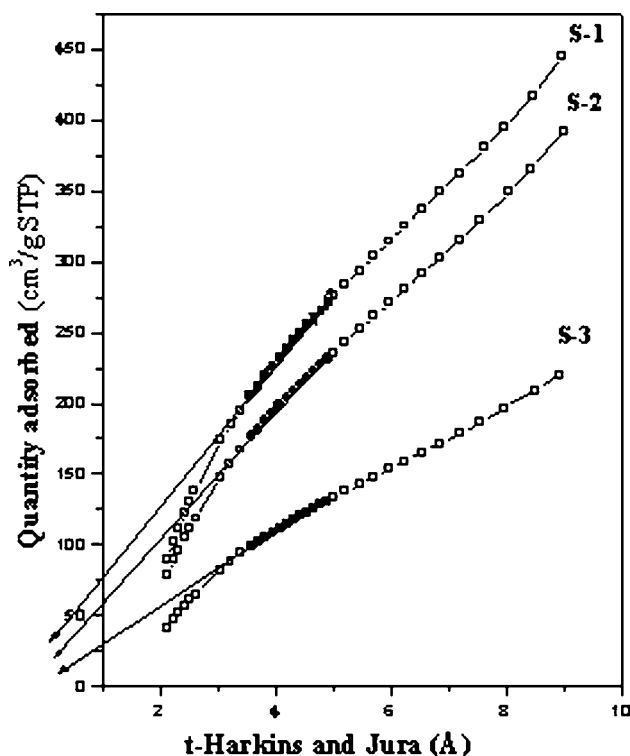


**Fig. 4**  $t$ -plot curve for the samples at ageing temperatures 100, 120 and 130°C

a hexagonal pattern.  $S_p$  and  $V_p$  are the surface area and pore volume of mesopores. The  $p/p_0$  position of the inflection point in isotherms is correlated to the diameter of the mesopore; small pores are filled at low pressures, large pores at higher pressures. The shift in  $p/p_0$  values with increase of temperature is due to the increase in pore diameter, which is in accordance with the Kelvin equation. In S-1 the  $p/p_0$  is 0.62, which shifts to 0.69 and 0.71 at higher temperatures (Fig. 2a). Higher temperatures or longer reaction time result in large pore sizes and thinner silica walls [28]. The micelle of the tri-block copolymer P123 in acidic solution consists of a core and a shell formed by the hydrophobic and hydrophilic parts, respectively. The micelle core radius depends upon the temperature of the aqueous solution [29]. In acid solution the hydrophilic EO moieties are expected to interact with the protonated silica by the ( $S^0H + X - I +$ ) mechanism and thus be closely associated with the inorganic wall. This interaction decides the microporosity of the material. Increasing the temperature results in increased hydrophobicity of the EO block moiety and therefore decreases, on average the lengths of the EO segments that are associated with the silica wall. This tends to increase the hydrophobic volumes of the surfactant aggregates resulting in the increased pore sizes in SBA-15 materials prepared and at the same time decreases the microporosity [30–32]. It is well known that the BJH

**Table 2** Physico chemical properties of pure silica of various pore dimensions and immobilized silica for the equilibrium loading of enzymes

Sample	BET surface area ( $S$ ) ( $\text{m}^2\text{g}^{-1}$ )	Pore diameter ( $W$ ) ( $\text{\AA}$ )	Micropore area ( $\text{m}^2\text{g}^{-1}$ )	Micropore vol ( $\text{cm}^3\text{g}^{-1}$ )	Pore volume ( $V$ ) ( $\text{cm}^3\text{g}^{-1}$ )	( $WS_p/V_p$ ) (nm)
S-1	856	63	113	0.056	1.35	3.6
S-2	734	74	90	0.044	1.41	3.5
S-3	515	84	41	0.020	1.14	3.6
S-1e <sub>1</sub>	544	60	–	–	1.19	–
S-2e <sub>1</sub>	277	62	–	–	0.49	–
S-3e <sub>1</sub>	355	70	–	–	0.98	–

method under estimate the pore size for a micro-mesomaterial. Methods based on the Kelvin equation (e.g., BJH method) are linked to the pore condensation phenomena, i.e., this is applicable for mesopore size analysis, but fail to describe the pore filling of micropores and even narrow mesopores in a correct way. In this work as the ageing was done at higher temperatures, the microporosity was reduced. Therefore, the BJH approach is reliable and the results from BJH are agreeable with the observed HRTEM results. The maximum in the PSD was taken as the pore diameter and it has close agreement with the pore diameter from the desorption branch of isotherm. The pore size distribution for S-1, S-2, and S-3 from BJH is shown in Fig. 3.

The drastic lowering of specific pore volume and surface area after immobilization is tentatively attributed to the tight packing of  $\alpha$ -amylase molecules in the pores of these materials (Table 2). As shown in Fig. 2b, the  $p/p_0$  values are suddenly lowered indicating pore blockage [11–13]. In S-2e (100 mg enzyme/g of support) and S-2e<sub>1</sub> (equilibrium adsorption) the amount of nitrogen adsorbed decreases systematically (Fig. 2b) with increasing enzyme loading due to the immobilization of biomolecules inside the pore channels of SBA-15 support. Nevertheless the difference between pore sizes without and with enzyme is hardly significant, and it does not justify the presence of protein inside the pore channels. For the equilibrium adsorption of enzymes on S-2, the surface area was reduced from 734 to 277  $\text{m}^2/\text{g}$ . The narrow, tight pore size distribution of S-2 confirms the ordered SBA-15 with pore diameter 74  $\text{\AA}$

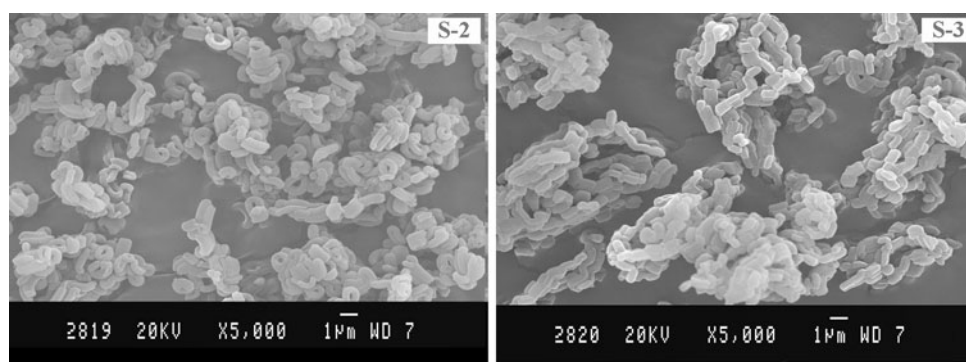
which is optimum for the immobilization of  $\alpha$ -amylase ( $35 \times 40 \times 70 \text{\AA}$ ).

### 3.3 Scanning electron microscopy

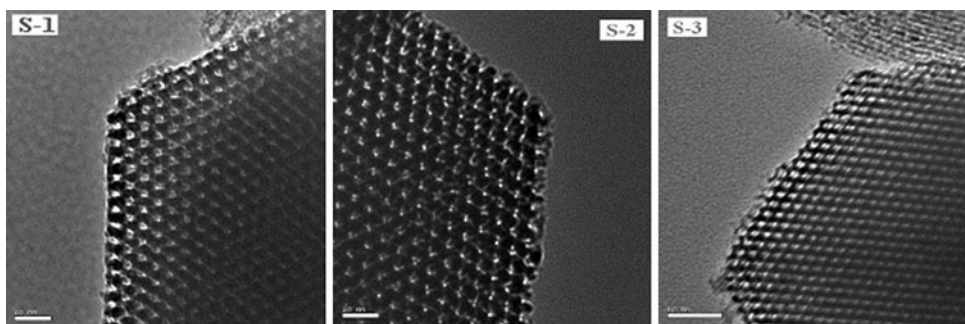
The SEM pictures of S-2 and S-3 synthesized having different particle size is shown in Fig. 5. Large fibrous structures are observed at higher temperatures. Similar SEM images were reported by other authors [33]. SBA-rods agglomerate and grow into large fibers when silica samples are subjected to higher temperature and time within the autoclave. The decrease in surface area with temperature supports this observation. The SBA-rods are  $\sim 1\text{--}2 \mu\text{m}$  in length and  $\sim 0.5 \mu\text{m}$  in diameter. The synthesis at  $130^\circ\text{C}$  is less favorable for protein adsorption because when the silica rods grow into long fiber many of the pore openings might be blocked as seen from images. After adsorption a similar morphology is observed indicating that the overall structure is maintained even after immobilization.

### 3.4 High resolution transmission electron microscopy

Figure. 6 presents HRTEM micrographs of the samples with various pore sizes. The images were recorded along two different crystallographic directions, with the incident electron beam parallel and perpendicular to the direction of main channels of SBA-15. These images show well-ordered hexagonal arrays of mesopores with one-dimensional channel, indicating the 2D hexagonal mesostructure

**Fig. 5** SEM images of samples at 120 and  $130^\circ\text{C}$ , respectively

**Fig. 6** HRTEM of samples at different temperatures 100, 120 and 130°C



characteristic of SBA-15 materials [34]. All the pore channels are highly uniform, regular and ordered. The pores of the rod-like sub-particles run parallel to the long axis of the rod. Comparing the pore sizes of the three samples (S-1, S-2 and S-3) the increase in pore size with temperature is evident and is in agreement with the data from pore size distribution. The pore size at 100°C was  $\sim 6\text{--}7$  nm and it is increased to  $\sim 7\text{--}8$  nm with increase in temperature. The decrease in pore wall thickness is also evident from the images and agrees with the data earlier calculated.

#### 4 Protein adsorption studies

Several reports describe the use of mesoporous molecular sieves to immobilize proteins. The adsorption of enzymes on mesoporous silica is determined by several factors. The influencing factors may include the experimental conditions such as the temperature, pH of the buffer solutions and the material properties such as the size of enzymes and nanopores, the composition, mesostructure and morphology of mesoporous materials. Balkus et al. [8] have studied the immobilization of enzymes with different sizes on MCM-41, MCM-48 and SBA-15. They suggested that the loading efficiency depends on the size of the enzyme and the pore size of the adsorbent, and indicated that the immobilization process takes place in the mesopores. Furthermore, they have found that the proteins retain their activity after adsorption. Takahashi et al. [6] studied the adsorption of horseradish peroxidase and subtilisin on FSM-16, MCM-41 and SBA-15 and found that the amount of adsorption on MCM-41 and FSM-16 is higher compared to SBA-15. In contrast, Yiu et al. [35] have recently studied the immobilization of trypsin on MCM-41, MCM-48 and SBA-15, and reported that the amount of trypsin adsorbed depends on the pore diameter of the adsorbent and that SBA-15 showed the maximum amount of trypsin adsorption. Most of the authors have compared the effect of pore size with different silica materials like MCM-41 and SBA-15. The effect of pore size on the rate of adsorption can be compared only if the same material with different pore sizes is taken. The adsorption

property will differ with the structural framework of silica. Several authors have varied the pore size of SBA-15 using pore regulating agents like TMB (tri methyl benzene) and the effect of pore size on rate of adsorption of different properties was studied. Katiyar et al. [36] studied the adsorption of enzymes of various dimensions in SBA-15 materials of various pore sizes prepared using PST and TMB. They have concluded that the adsorption capacity and rate of adsorption is dependant on the solution pH, protein and pore size. Regulating the pore using TMB does not give well ordered structures. In the present work, well ordered mesoporous silica material of similar framework with various pore sizes was synthesized hydrothermally.

The kinetics of  $\alpha$ -amylase adsorption on SBA-15 samples at pH 6 is shown in Fig. 7. Since  $\alpha$ -amylase has dimensions of  $35 \times 40 \times 70$  Å it is expected that the protein has access to the pores of all samples prepared at 120 and 130°C. High equilibrium capacity ( $>220$  mg/g) in a short time of  $\sim 40$  min indicates that the huge pore volume of S-2 with sufficient pore opening allows the complete penetration of enzyme molecules well within the pore. For S-1, the rise to saturation is much slower than for S-2 and S-3; for S-2 the rate curve is close to rectangular,

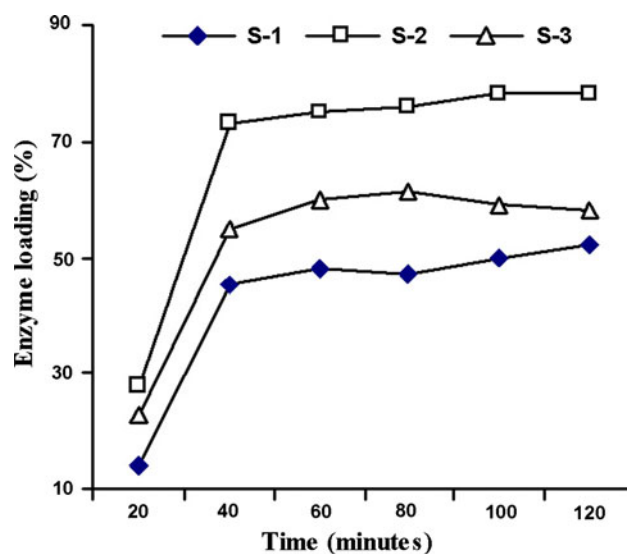


**Fig. 7** Rate of adsorption of enzymes on various supports at pH 6

indicating very good access to the pore. This might be due to the ordered nature of S-2 with optimum pore size. But from the adsorption studies it is evident that optimum pore size alone does not enhance adsorption rate. The loading with S-3 sample was low ( $<165$  mg) even though the pore size was much larger of  $84 \text{ \AA}$ . The low loading of enzymes on S-3 is definitely due to pore blockage during the growth of SBA-15 rods into larger fibers at higher autoclave temperature. In SBA-15 type mesoporous silica the morphology and particle size plays an important role in the immobilization ability [37]. Raising the temperature to  $130^\circ\text{C}$  has decreased the surface area considerably even though the pore size increased to  $84 \text{ \AA}$ . This decrease might be due to the condensation of silica at a faster rate during its growth into long fibers as envisaged from SEM images. This growth of silica, block the free adsorption of biomolecules inside the channels. Zhao et al. [38] has reported that rod-like SBA-15 with straight channels ( $1\text{--}2 \mu\text{m}$  in length) possesses the fastest adsorption rate reaching  $200 \text{ mg/g}$  within 10 min at  $25^\circ\text{C}$  and the largest immobilization amount of  $500 \text{ mg/g}$  among all reported mesoporous silicas. By carefully controlling the morphology of mesoporous silicas, it is revealed that silica with smaller particle sizes possess more entrances to entrap enzymes than conventional mesoporous silicas with larger particle sizes, which leads to much improved bioimmobilization abilities of mesoporous silicas. So a control of morphology while the synthesis is essential for good adsorption property. The accessible surface area for protein adsorption is not similar for the two materials S-2 and S-3 in spite of the higher pore diameter and hence the enzyme loading is also different. It is also noticeable that the pore volume after immobilization decreased drastically from  $1.41$  to  $0.49 \text{ cm}^3 \text{ g}^{-1}$  in the case of S-2 but the decrease was not sharp for S-3 ( $1.14\text{--}0.98 \text{ cm}^3 \text{ g}^{-1}$ ). Another reason for low loading is that the total pore volume decreases as the pore diameter increases, so that the surface area which can provide active sites for the enzyme immobilization also decreases. Vinu et al. [39] has reported that the amount of adsorbed cytochrome *c* is dependant on pore volume which decreases with increase in pore diameter. This result suggests that pore volume could be more important factor than pore diameter. To study the effect of pore structure we have also compared the enzyme loading on the cheap support natural rice husk silica with no regular pore structure. The acid leached rice husk silica has a surface area of  $242 \text{ m}^2/\text{g}$  and 27% of the total surface area was occupied at equilibrium adsorption while it is 67% for mesoporous silica with regular pore structure (S-2). The irregular pores with low dimension do not allow the enzyme molecules to penetrate in.

Besides the pore size of the mesoporous silica, the solution pH is another important factor to be considered for

enzyme immobilization. The forces binding proteins to hydrated silica surfaces include hydrogen bonding, hydrophobic interactions and electrostatic protein-surface interactions. The sign of the overall charge on a surface can readily be predicted on the basis of the isoelectric point pI (the pH at which the overall charge is zero). This pI value of a protein molecule depends on the balance of surface functional groups which may have opposite charges. When the adsorption is performed at a pH lower than the pI of the enzyme (but higher than pI of the silica) the protein will be positively charged. The isoelectric point of the silica surface of mesoporous material is around 2 hence the adsorbent surface is negatively charged at pH above 2. The greater the positive charge on the enzyme, the stronger the attraction between protein and surface, but stronger the repulsion between adsorbed molecules. According to Su et al. [40], surface adsorption capacities of proteins are found to vary with the pH of adsorption according to a bell-curve, the maximum of which occurs at the isoelectric point of protein. It therefore follows that by judicious variation of the pH; proteins could be adsorbed selectively and desorbed by changing the pH. Previous study on the adsorption of biomolecules on pure silica materials showed that strong electrostatic interactions between the surface silanol groups and the surface charge of protein molecules were a critical factor [41, 42]. According to Sakaguchi and coworkers [43] the driving forces for the adsorption of Hb include hydrophobic interactions, electrostatic repulsion and attraction, the intramolecular cohesive attraction and repulsion. Vinu et al. provide systematic researches on protein adsorption onto mesoporous materials. The influence of the solution pH on the adsorption of cytochrome *c* and lysosome was studied by his group [44]. Typical results of adsorption of hen egg white lysozyme and horse heart cytochrome *c* onto three mesoporous silica materials obeyed Langmuir-type behavior. The results revealed that the adsorption of lysozyme was determined by electrostatic and hydrophobic interactions. The studies on the adsorption of biomaterials on the mesoporous carbon reveal that hydrophobic interaction between guest molecules and surface of the mesoporous materials is an important parameter which controls the amount of biomaterials adsorption [45].

The effect of pH on adsorption was studied at room temperature by varying the pH in the range 4–8 on the size matching pore (Fig. 8). It can be seen that the monolayer adsorption capacity of S-2 significantly changes depending on the solution pH. The isotherms measured in the pH range 4–6 show a sharp initial rise, suggesting a high affinity between amylase and the adsorbent surface. Finally, the isotherms reach a plateau. The amount adsorbed increases from pH 4–6 and further decreases. At pH 8, adsorption is very low and it takes longer time to reach equilibrium. The maximum adsorption at pH 5–6 can be

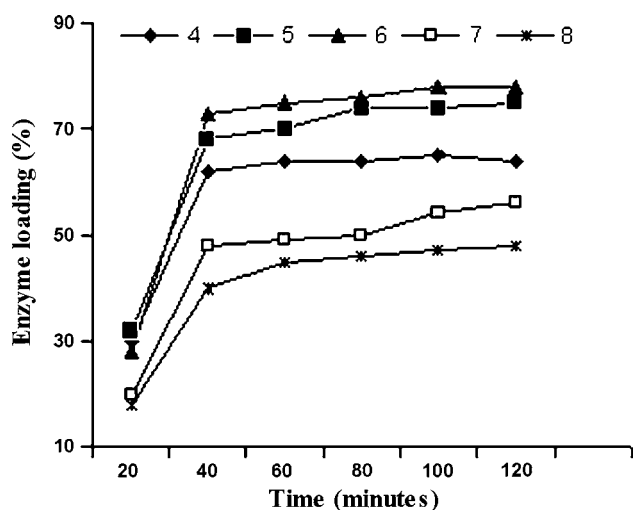


**Fig. 8** Adsorption isotherms of  $\alpha$ -amylase on SBA-15 of pore size 74 Å at various pH

explained as follows; near the isoelectric point the net charge of the protein is low and the coulombic repulsive force between the molecules is minimal. Consequently a closer packing of the protein molecules is possible and the monolayer capacity increases. It is observed that there is a large reduction in the amount of  $\alpha$ -amylase adsorbed on silica at pH below and above pI. It is a well known fact that the protein molecule is positively charged at a pH below pI and negatively charged at a pH above pI. When the solution pH is decreased to 4, the net positive charges of the amylase molecule start to increase and so does the lateral repulsion between protein molecules. As a consequence, the protein molecule requires more space and the monolayer capacity decreases. When the solution pH is increased to 8 the surface of the  $\alpha$ -amylase molecule become negatively charged and enhances the electrostatic repulsion between protein molecules and the silica surface. The maximum adsorption occurs at pH 6 which is close to the isoelectric point of  $\alpha$ -amylase (5.5).

## 5 Conclusions

Highly ordered mesoporous SBA-15 with different pore sizes has been synthesized hydrothermally. The materials were characterized thoroughly before and after adsorption. The immobilization behaviour of  $\alpha$ -amylase in mesoporous molecular sieve with different pore sizes and buffer concentrations has been studied. The  $N_2$  adsorption–desorption studies confirm the entrapment of enzymes inside the pore. For a given pore diameter the amount of enzyme adsorbed depends on the pH of the medium and maximum adsorption is around the isoelectric point of enzyme. For a given pH the amount adsorbed increases with pore volume and

for maximum adsorption optimum pore size with controlled morphology is essential.

## References

1. A. Corma, *Chem. Rev.* **97**, 2373 (1997)
2. H.X. Zhou, K.A. Dill, *Biochem.* **40**, 11289 (2001)
3. S. Sotiropoulou, V. Vamvakaki, N.A. Chaniotakis, *Biosens. Bioelectron.* **20**, 1674 (2005)
4. D. Zhao, J. Feng, Q. Huo, N. Melosh, G.H. Fredrickson, B.F. Chmelka, G.D. Stucky, *Science* **279**, 548 (1998)
5. D. Zhao, Q. Huo, J. Feng, B.F. Chmelka, G.D. Stucky, *J. Am. Chem. Soc.* **120**, 6024 (1998)
6. H. Takahashi, B. Li, T. Sasaki, C. Miyazaki, T. Kajino, S. Inagaki, *Micropor. Mesopor. Mater.* **44/45**, 755 (2001)
7. W.H. Zhang, L. Zhang, J. Xiu, Z. Shen, Y. Li, P. Ying, C. Li, *Micropor. Mesopor. Mater.* **89**, 179 (2006)
8. J.F. D'Áz, K.J. Balkus Jr., *J. Mol. Catal. B* **2**, 115 (1996)
9. J. Deere, E. Magner, J.G. Wall, B.K. Hodnett, *Catal. Lett.* **85**, 19 (2003)
10. H.H.P. Yiu, P.A. Wright, *J. Mater. Chem.* **15**, 3690 (2005)
11. H. Takahashi, B. Li, T. Sasaki, C. Miyazaki, T. Kajino, S. Inagaki, *Chem. Mater.* **12**, 3301 (2000)
12. M. Hartmann, *Chem. Mater.* **17**, 4577 (2005)
13. O. Martin, L. Averous, *Polymer* **42**, 6209 (2001)
14. R. Reshmi, G. Sanjay, S. Sugunan, *Catal. Commun.* **8**, 393 (2007)
15. S. Gopinath, S. Sugunan, *Appl. Clay Science* **35**, 67 (2007)
16. G. Sanjay, S. Sugunan, *J. Porous. Mater.* (In Press)
17. P. Pandya, R.V. Jasra, P.N. Bhatt, *Micropor. Mesopor. Mater.* **77**, 67 (2005)
18. A. Sousa, E.M.B. Sousa, *J. Non-crystalline Solids* **352**, 3451 (2006)
19. B. Marler, U. Oberhagemann, S. Vortmann, H. Gies, *Micropor. Mesopor. Mater.* **6**, 375 (1996)
20. W. Hammond, E. Prouzet, S.D. Mahanti, T.J. Pinnavaia, *Micropor. Mesopor. Mater.* **27**, 19 (1999)
21. A. Vinu, M. Miyahara, K. Ariga, *J. Phys. Chem. B.* **109**, 6436 (2005)
22. K.S.W. Sing, D.H. Everett, R.A.W. Haul, L. Moscow, R.A. Pierotti, J. Rouquerol, T. Siemieniowska, *Pure Appl. Chem.* **57**, 603 (1985)
23. B.L. Newalkar, S. Komarneni, *Chem. Mater.* **13**, 4573 (2001)
24. M. Hartmann, A. Vinu, *Langmuir* **18**, 8010 (2002)
25. M. Kruk, M. Jaroniec, C.H. Ko, R. Ryoo, *Chem. Mater.* **12**, 1961 (2000)
26. R. Ryoo, C.H. Ko, M. Kruk, V. Antochshuk, M. Jaroniec, *J. Phys. Chem. B.* **104**, 11465 (2000)
27. H.J. Shin, R. Ryoo, M. Kruk, M. Jaroniec, *Chem. Commun.* 349 (2001)
28. A. Galarnau, H. Cambon, T. Martin, L.-C. de Menorval, D. Brunel, F.D. Renzo, F. Fajula, *Stud. Surf. Sci. Catal.* **141**, 395 (2002)
29. M. Thommes, R. Kohn, M. Froba, *Appl. Surf. Sci.* **196**, 23 (2002)
30. K. Mortensen, J.S. Pedersen, *Macromolecules* **26**, 805 (1993)
31. K. Mortensen, W. Brown, *Macromolecules* **26**, 4128 (1993)
32. G. Wanka, H. Hoffmann, W. Ulbricht, *Macromolecules* **27**, 4145 (1994)
33. C.H. Lei, Y. Shin, J. Liu, E.J. Ackerman, *J. Am. Chem. Soc.* **124**, 11242 (2002)
34. A.S.M. Chong, X.S. Zhao, A.T. Kustedjo, S.Z. Qiao, *Micropor. Mesopor. Mater.* **72**, 33 (2004)
35. H.H.P. Yiu, P.A. Wright, N.P. Botting, *Micropor. Mesopor. Mater.* **44–45**, 763 (2001)

36. L. Ji, A. Katiyar, N.G. Pinto, M. Jaroniec, P.G. Smirnioti, *Micropor. Mesopor. Mater.* **75**, 221 (2004)
37. J. Fan, J. Lei, L. Wang, C. Yu, B. Tu, D. Zhao, *Chem. Commun.* 2140 (2003)
38. J. Lei, J. Fan, C. Yu, L. Zhang, S. Jiang, B. Tu, D. Zhao, *Micropor. Mesopor. Mater.* **73**, 121 (2004)
39. A. Vinu, V. Murugesan, M. Hartmann, *J. Phys. Chem. B* **108**, 7323 (2004)
40. T.J. Su, J.R. Lu, R.K. Thomas, Z.F. Cui, J. Penfold, *J. Colloid Interface Sci.* **203**, 419 (1998)
41. J.M. Kislner, G.W. Stevens, A.J. OConnor, *Mater. Phys. Mech.* **4**, 89 (2001)
42. S.Z. Qiao, C.Z. Yu, W. Xing, Q.H. Hu, H. Djojoputro, G.Q. Lu, *Chem. Mater.* **17**, 6172 (2005)
43. M. Matsui, Y. Kiyozumi, T. Yamamoto, Y. Mizushina, F. Mizukami, K. Sakaguchi, *Chem. Eur. J.* **7**, 1555 (2001)
44. A. Vinu, V. Murugesan, O. Tangemann, M. Hartmann, *Chem. Mater.* **16**, 3056 (2004)
45. M. Hartmann, A. Vinu, G. Chandrasekar, *Chem. Mater.* **17**, 829 (2005)